Ca^{2+} Binding in the Active Site of HincII: Implications for the Catalytic Mechanism[†,‡]

Christopher Etzkorn and Nancy C. Horton*

Department of Biochemistry and Molecular Biophysics, University of Arizona, Tucson, Arizona 85721

Received May 17, 2004; Revised Manuscript Received August 16, 2004

ABSTRACT: The 2.8 Å crystal structure of the type II restriction endonuclease HincII bound to Ca^{2+} and cognate DNA containing GTCGAC is presented. The DNA is uncleaved, and one calcium ion is bound per active site, in a position previously described as site I in the related blunt cutting type II restriction endonuclease EcoRV [Horton, N. C., Newberry, K. J., and Perona, J. J. (1998) *Proc. Natl. Acad. Sci. U.S.A. 95* (23), 13489−13494], as well as that found in other related enzymes. Unlike the site I metal in EcoRV, but similar to that of PvuII, NgoMIV, BamHI, BglII, and BglI, the observed calcium cation is directly ligated to the *pro*-S_p oxygen of the scissile phosphate. A calcium ion-ligated water molecule is well positioned to act as the nucleophile in the phosphodiester bond cleavage reaction, and is within hydrogen bonding distance of the conserved active site lysine (Lys 129), as well as the *pro*-R_p oxygen of the phosphate group 3′ of the scissile phosphate, suggesting possible roles for these groups in the catalytic mechanism. Kinetic data consistent with an important role for the 3′-phosphate group in DNA cleavage by HincII are presented. The previously observed sodium ion [Horton, N. C., Dorner, L. F., and Perona, J. J. (2002) *Nat. Struct. Biol. 9*, 42−47] persists in the active sites of the Ca^{2+}-bound structure; however, kinetic data show little effect on the single-turnover rate of DNA cleavage in the absence of Na^+ ions.

Nearly all enzymes which cleave duplex DNA do so in a divalent cation-dependent manner (*1*, *2*), including those involved in modifying DNA supercoiling (*3*, *4*), DNA repair (*5*−*8*), transposition (*9*, *10*), recombination (*11*−*13*), homing (*14*), and bacterial immunity (*1*, *15*−*20*). Models of the catalytic mechanisms of many of these enzymes have been derived from three-dimensional X-ray crystallographic structures, as well as from mutagenic and biochemical analyses. Many models involve variations of the two-metal ion mechanism originally proposed for the 3′−5′ exonuclease activity of *Escherichia coli* DNA polymerase I (*21*). Important differences in the details of the proposed mechanistic models may be either a result of artifacts of the studies used to derive them or, alternatively, due to real differences in the mechanisms utilized by different enzymes.

The roles of divalent cations in the cleavage mechanism of duplex DNA have been intensely studied in the type II restriction endonucleases (*15*−*20*, *22*−*25*). Type II restriction endonucleases typically utilize Mg^{2+} as the *in vivo* divalent cation cofactor, but will also cleave DNA, albeit with less sequence specificity, in the presence of Mn^{2+} or Co^{2+} (*26*). Binding studies using the gel shift assay, filter binding, and fluorescence polarization anisotropy have determined that substitution of Ca^{2+} for Mg^{2+} confers specific and tight binding while preventing cleavage of the DNA (*27*−*29*), allowing the structural analysis of enzyme−DNA complexes with divalent cations prior to reaction.

Structural studies of the divalent cation-dependent phosphoryl transfer mechanism of type II restriction endonucleases include EcoRV, BamHI, PvuII, BglI, EcoRI, NgoMIV, and BglII (*1*, *15*−*20*). Many of the important details of these mechanisms differ. The mechanisms proposed for EcoRI and BglII utilize only a single divalent cation. Of those that involve at least two divalent cations, stabilization of the leaving group is performed either by direct ligation in some mechanistic models or by protonation of the leaving group via a divalent cation-bound water molecule in others. Mechanistic models also appear to differ in the direct ligation of the scissile phosphate, involving either both divalent cations or, in some cases, only one of the two. Finally, an unresolved issue in many mechanistic models is the identity of, and even requirement for, a catalytic base accepting the proton from the attacking water molecule. Only the mechanism proposed for BamHI (*17*), as well as the earlier substrate-assisted catalysis mechanism of EcoRV (*30*), involves general base catalysis. Computational studies have suggested that proton transfer to water may be more favorable than to a general base in the type II restriction endonuclease BamHI (*31*).

A lack of strict conservation of the active site residues has made the case for mechanistic divergence among the type II restriction endonucleases very strong (*17*, *18*). However, the extent and details of this divergence among all endonucleases are not known. All type II restriction endonucleases structurally characterized to date display the same basic fold involving a five-stranded β-sheet flanked by α-helices. The common fold and function of these enzymes have been used as evidence of a common evolutionary origin. Similarly, detailed structural comparisons

[†] This work was supported by NIH Grant 1 R01 GM066805-01A1.

[‡] Coordinates have been deposited in the Protein Data Bank as entry 1TW8.

* To whom correspondence should be addressed. Telephone: (520) 626-3828. Fax: (520) 626-9288. E-mail: nhorton@u.arizona.edu.

10.1021/bi0490082 CCC: $27.50
Published on Web 10/02/2004

Chart 1

```
16mer top          5'HEX-GGG CCG GTC|GAC CAA C3'
16mer bottom           3'CCC GGC CAG|CTG GTT G-HEX5'
```

imply a closer evolutionary relationship between enzymes with similar cut patterns (*32*, *33*); blunt cutting enzymes EcoRV, PvuII, and HincII share topological features not present in 5′ sticky cutting enzymes EcoRI, BamHI, MunI, BglII, and NgoMIV, and vice versa. If mechanistic divergence exists, then mechanisms of more closely related enzymes may share similarities that differ from more distantly related enzymes.

While no studies of DNA-cleaving enzymes have implicated monovalent cations directly in the catalytic mechanisms, potassium ions have been located in the structure of a heat shock protein and shown to be important for its activity (*34*, *35*). In addition, monovalent cations may also be involved in other enzymatic phosphotransfer mechanisms (*36*, *37*). A sodium ion was found in the original structure of HincII bound to cognate DNA (*38*) at the scissile phosphate; however, its role in the catalytic mechanism was not clear, and its binding was suspected to be a result of the absence of bound divalent cations.

Presented herein is the 2.8 Å crystal structure of *Hinc*II bound to cognate DNA derived from crystals soaked in a buffer containing 50 mM Ca^{2+}. HincII is a type II restriction endonuclease which binds and cleaves duplex DNA containing GTY|RAC (where | denotes the cleavage site, Y is either pyrimidine, and R is either purine) leaving blunt ends (*39*). The DNA recognition sequence contains degeneracy in the center two base pairs, allowing any combination of pyrimidine-purine sequences (i.e., TA, TG, CG, or CA). No global conformational changes are seen between this and the previously reported HincII structure; however, two new features are noted. First, approximately 12 residues of each subunit previously found to be disordered are ordered in the structure presented here. In addition, a different packing interaction between neighboring DNA duplexes has been modeled.

The binding of Ca^{2+} to HincII was investigated in an effort to improve the understanding of the divalent cation DNA cleavage mechanism of HincII, as well as the possible divergence of mechansims among type II restriction endonucleases. In the structure presented here, one calcium ion is found per active site directly ligated to the scissile phosphate, as well as to a water molecule in a favorable position for performing nucleophilic attack. The previously identified sodium ion persists in the current structure; however, we show here that single-turnover rates of cleavage of DNA by HincII are not diminished, but rather slightly increased, with the replacement of Na^+ with NH_4^+.

Directly ligated to the active site Ca^{2+} ion is a water molecule in a good position for nucleophilic attack in the phosphoryl transfer reaction. The "attacking" water molecule is within hydrogen bonding distance of both the active site lysine, Lys 129, and a nonesterified oxygen of the downstream (3′) phosphate. The lysine is part of the restriction endonuclease motif, $PDX_n(D/E)X\mathbf{K}$; however, the function of this motif residue has been unclear. Possible roles for this residue will be discussed. Studies of substrates missing the phosphate 3′ to the scissile phosphate show a requirement of this group for DNA cleavage by some type II restriction endonucleases (*30*). Here we present binding and kinetic data supporting the importance of the 3′-phosphate to DNA cleavage rates, but not binding affinity, of HincII. The structural features of the Ca^{2+} binding site provide insight into the catalytic mechanism of HincII, and comparison to mechanisms proposed for other type II restriction endonucleases provides insight into the issue of mechanistic divergence.

MATERIALS AND METHODS

Crystallization, Diffraction Data Collection, and Structure Refinement. The purification and crystallization protocol for HincII with cognate DNA (GCCGGTCGACCGG) has been described previously (*40*). A cocrystal of HincII bound to this DNA was soaked in a solution of 25% PEG 4K, 0.1 M acetate (pH 5.5), 0.3 M NaCl, and 50 mM $CaCl_2$ for 2 days at 17 °C, cryoprotected with a solution of 25% PEG 4K, 0.1 M acetate (pH 5.5), 0.3 M NaCl, and 30% glycerol, and then flash-frozen in liquid nitrogen. X-ray diffraction amplitudes were measured using synchrotron radiation at Stanford Synchrotron Radiation Laboratory (SSRL) beamline 9-1. Determination of the orientation matrix, integration, scaling, and merging of data were performed with MOSFLM (*41*) and SCALA (*42*). The structure was phased using a previously determined HincII−DNA cocrystal structure (Protein Data Bank entry 1KC6), with all solvent molecules removed from the initial model. Refinement was performed with CNS (*43*), and model building utilized XtalView (*44*).

Calculation of Omit Difference Maps. Near the final stages of refinement, simulated annealing omit maps were made using the CNS protocol sa_omit_map.inp using a starting temperature of 2000 K and a step size of 25 K, where atoms within a 5−7 Å radius are excluded from the simulated annealing protocol. Maps were drawn using Bobscript (*45*), a modified version of Molscript (*46*), and Raster 3D (*47*).

DNA Substrates. Substrates for the binding and kinetic measurements include 5′-hexachlorofluorescein (HEX[1])-labeled DNA (HincII cleavage sites indicated by | in Chart 1) and DNA 5′ end labeled with ^{32}P using T4 polynucleotide kinase (Fermentas, Hercules, CA) and [γ-^{32}P]ATP (MP Biomedicals, Irvine, CA), desalted in Micro Bio-spin 6 columns with P-polyacrylamide P-6 gel (Bio-Rad, Hercules, CA) (Chart 2).

The DNA was purchased commercially and purified by reverse phase HPLC. The HincII recognition sequence is underlined, and the full-length 16mer and 32mer duplexes were assembled as shown. The duplex DNA substrates containing the HincII recognition sequence missing the phosphate 3′ from the scissile phosphate were prepared using one full-length 32mer oligonucleotide, and the corresponding complementary pieces; i.e., the full-length top 32mer oligonucleotide was annealed with the two 32mer bottom pieces, and the full-length 32mer bottom piece was annealed to the

[1] Abbreviations: HEX, hexachlorofluorescein; PAGE, polyacrylamide gel electrophoresis.

Chart 2

```
32mer top              5′CC GGG CCC AAA CCG GTC|GAC CAA AAA AAG GCG 3′
32mer bottom           3′GG CCC GGG TTT GGC CAG|CTG GTT TTT TTC CGC 5′

32mer top piece 1      5′CC GGG CCC AAA CCG GTC|G
32mer top piece 2                              5′AC CAA AAA AAG GCG3′

32mer bottom piece 1   3′GG CCC GGG TTT GGC CA
32mer bottom piece 2                        3′G|CTG GTT TTT TTC CGC 5′
```

two 32mer top pieces. Only the full-length oligonucleotides as well as 32mer top piece 1 and 32mer bottom piece 2 were radiolabeled. Cleavage of the radiolabeled intact 32-nucleotide top strand results in a radiolabeled 17mer, while cleavage of the radiolabeled bottom piece 2 16mer results in a radiolabeled 15mer. Cleavage of the radiolabeled intact 32-nucleotide bottom strand results in a radiolabeled 15mer, while cleavage of the radiolabeled top piece 1 18mer results in a radiolabeled 17mer. Therefore, the substrates have been designed so that cleavage products can be easily distinguished from the parent oligonucleotides. Verification of full duplex formation of the substrates missing the 3′-phosphate was performed by native gel electrophoresis, using the intact duplex 32mer as a standard (Figure 1a).

Single-Turnover Cleavage Rate Measurements. Duplex oligonucleotides were incubated at 10 nM with 110 nM HincII in the reaction mixtures for single-turnover cleavage rate measurements. The reactions were carried out in a solution composed of 50 mM Bis-Tris propane (pH 7.5), 10 mM $MgCl_2$, 1 mM DTT, and 0.1 mg/mL BSA mixed with a solution containing 50 mM Bis-Tris propane (pH 7.5), 500 mM NaCl or NH_4Cl, 10 mM $MgCl_2$, 1 mM DTT, and 0.1 mg/mL BSA to a final conductivity of a solution containing 50 mM Bis-Tris propane (pH 7.5), 140 mM NaCl, 1 mM DTT, and 0.1 mg/mL BSA. In the case of the reactions conducted in the presence of NH_4Cl (and absence of NaCl), both the HincII protein and DNA were extensively dialyzed against the reaction buffer prior to the cleavage reaction measurements. The buffer was carefully made without the use of Na^+-containing reagents. The dialysis buffer was composed of 50 mM Bis-Tris propane (pH 7.5), 500 mM NH_4Cl, 10 mM $MgCl_2$, 0.1 mg/mL BSA, 1 mM DTT mixed with 50 mM Bis-Tris propane (pH 7.5), 10 mM $MgCl_2$, 0.1 mg/mL BSA, and 1 mM DTT to a conductivity (19.00 mS/cm) of 50 mM Bis-Tris propane (pH 7.5), 140 mM NaCl, 0.1 mg/mL BSA, and 1 mM DTT. Over the course of 72 h, 400 μL of HincII and 5 μL of 5′-HEX-labeled CG DNA were dialyzed against 500 mL of buffer, with six changes of the dialysis buffer. The enzyme was diluted 1:1 with glycerol and, along with the DNA, stored at −20 °C until it was needed.

Reactions were performed in triplicate and initiated by the rapid mixing of protein and DNA, each preincubated in reaction buffer at 37 °C, followed by incubation at 37 °C. Reactions were quenched at specific times after mixing using a KinTek RQF-3 Rapid Quench Flow instrument (KinTek Corp., Austin, TX) for the faster reactions (using the 16mer HEX-labeled substrates). Each reaction (in a volume of 225 μL) was quenched at times ranging from 0.5 to 120 s with an equal volume of quench solution (4 M urea, 40% formamide, and 50 mM EDTA). Slower reactions were performed by hand using a 100 μL total reaction volume, and reaction (in a volume of 10 μL) was quenched with 10 μL of quench solution at various times after initiation. The reaction solutions were overlaid with mineral oil to prevent evaporation. The quenched reactions were then run on a 16% acrylamide denaturing gel (containing 6 M urea) in 1× TBE [89 mM Tris, 89 mM boric acid, and 10 mM EDTA (pH 8.3)]. A Typhoon scanner (Molecular Dynamics, Sunnyvale, CA) was used to detect the HEX-labeled DNA directly in the gels, and radioactivity was measured using a storage phosphor image plate and the Typhoon scanner in the case of the ^{32}P-labeled DNA gels. The product bands were integrated using ImageQuant (Molecular Dynamics), and then plotted against the length of the reaction. The time courses of the intensities of the product bands were fit to a single exponential [$P = C(1 - e^{-kt})$]. Both the single-turnover rate constant k and the total amount of product C were fit by Kaleidagraph (Synergy, Reading, PA). All reported measurements are the result of at least three independent time courses.

Measurement of Dissociation Constants. The apparent dissociation constant K_D for dissociation of HincII from the various DNA substrates described above was measured by a gel shift assay (*28*, *48*−*51*). The binding buffer was composed of 50 mM Bis-Tris propane (pH 7.5), 5 mM $CaCl_2$, 1 mM DTT, and 0.1 mg/mL BSA mixed with a solution containing 50 mM Bis-Tris propane (pH 7.5), 500 mM NaCl, 5 mM $CaCl_2$, 1 mM DTT, and 0.1 mg/mL BSA to a final conductivity of a solution containing 50 mM Bis-Tris propane (pH 7.5), 140 mM NaCl, 1 mM DTT, and 0.1 mg/mL BSA. The DNA concentration used in all studies was 5.6×10^{-11} or 6.6×10^{-11} M, and protein concentrations varied from 5.5×10^{-11} to 2.0×10^{-7} M. Protein and DNA were incubated at 37 °C for 30 min, rapidly mixed with prewarmed loading buffer composed of binding buffer with 20% glycerol (without running dyes), and immediately loaded onto a 10% native PAGE gel. Loading of the gels took place while the gels were undergoing electrophoresis. The running buffer was composed of 89 mM Tris, 89 mM boric acid, and 5 mM $CaCl_2$ (pH 8.3). The gels were electrophoresed at 190 V and 4 °C with recirculation of the running buffer. Gels were autoradiographed using a storage phosphor image plate. The image plate was scanned using a Typhoon imager (Molecular Dynamics); band intensities were quantitated by densitometry using Imagequant (Molecular Dynamics), and data were fitted by nonlinear regression using Kaleidagraph (Synergy) and the equation

$$A = A_{min} + (A_{max} - A_{min})\{P_T + D_T + K_D - [(P_T + D_T + K_D)^2 - 4P_TD_T]^{1/2}\}/(2D_T)$$

where A represents the protein−DNA band intensity. Both A_{max} and A_{min} were fit in addition to K_D. The DNA concentration, D_T, was held constant, and P_T, the total protein

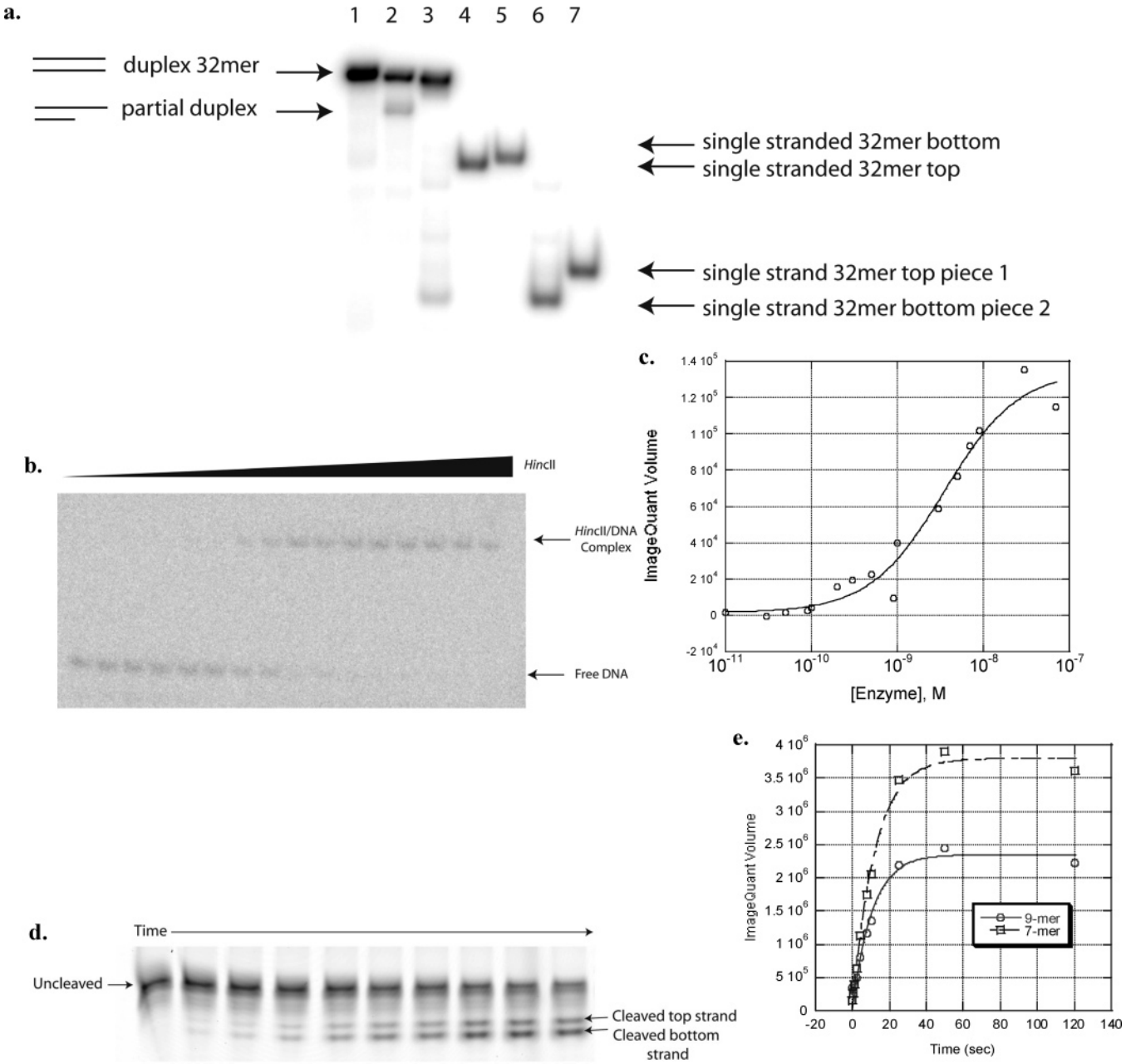

FIGURE 1: (a) Native PAGE of DNA substrates: lane 1, duplex 32mer composed of 32mer top and 32mer bottom; lane 2, duplex 32mer missing the phosphate 3′ of the scissile phosphate on the top strand [composed of 32mer bottom (radiolabeled), 32mer top piece 1 (radiolabeled), and 32mer top piece 2 (not radiolabeled)]; lane 3, duplex 32mer missing the phosphate 3′ of the scissile phosphate on the bottom strand [composed of 32mer top (radiolabeled), 32mer bottom piece 1 (not radiolabeled), and 32mer bottom piece 2 (radiolabeled)]; lane 4, single-stranded 32mer top; lane 5, single-stranded 32mer bottom; lane 6, single-stranded 32mer bottom piece 2; and lane 7, single-stranded 32mer top piece 1. (b) Autoradiogram of a gel shift experiment in which reaction mixtures containing 4.5×10^{-11} M ^{32}P-labeled DNA are incubated with increasing concentrations of HincII, and then electrophoresed using native PAGE. The positions of unbound DNA and DNA bound to HincII are as marked. (c) Fit of gel shift data in panel b to the binding equation given in Materials and Methods. (d) Scan of HEX-bound DNA in denaturing PAGE after incubation with HincII for specific time intervals under single-turnover conditions as described in Materials and Methods. The positions of cleaved and uncleaved DNA are as marked. (e) Fit of single-turnover cleavage data in panel d. The 9mer corresponds to cleavage of the top strand, and the 7mer corresponds to cleavage of the bottom strand.

concentration, varies with each measurement of *A*. Except where noted, the reported measurements are the result of three independent binding isotherms.

RESULTS

Overall Structure. The structure of wild-type HincII bound to DNA containing the sequence GTCGAC and Ca^{2+} has been refined at 2.8 Å to an R_{cryst} of 18.0% and an R_{free} of 28.6%. The asymmetric unit contains two dimers of HincII (1018 total residues) and two duplexes of DNA (52 total nucleotides), as well as 765 water molecules, six calcium ions, and four sodium ions. The overall structure of HincII bound to DNA containing the recognition sequence GTCGAC and Ca^{2+} is shown in Figure 2, superimposed on the HincII−DNA binary complex. No large conformational changes occur, and the two superimpose with a root-mean-square displacement of 0.42 Å among main chain atoms. The DNA is found uncleaved in the ternary complex, and also exhibits no large conformational changes. Two new general features are, however, seen in the structure described

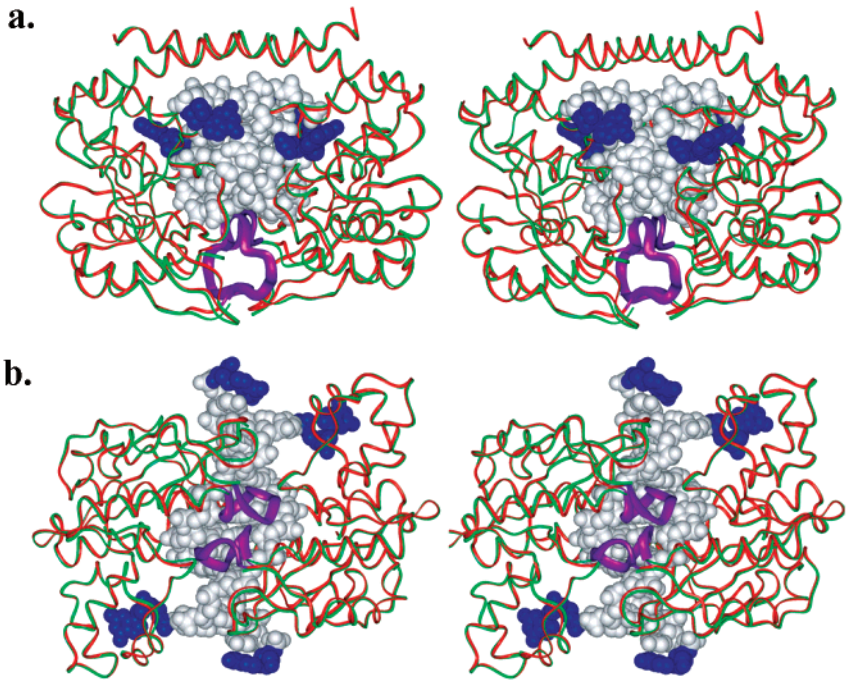

FIGURE 2: (a) Stereodiagram of a superposition of HincII bound to DNA (green) with the HincII−DNA−Ca^{2+} structure (red) shown as backbone ribbons. The linker regions (residues 22−33) of both subunits in the HincII−DNA−Ca^{2+} structure are shown in purple. The DNA from the HincII−DNA−Ca^{2+} structure is shown in space filling form in white (nucleotides 2−12) and blue (nucleotides 1 and 13). (b) Panel a rotated 90°.

herein, namely, the increased order in residues 22−33, or the linker region, of each subunit and a previously undetected overlap in base pairing at the ends of each oligonucleotide involved in lattice contacts (see below).

Ordering of Linkers. The region from residue 22 to 33 in each subunit of the previously published HincII−DNA structure was disordered and omitted from the final refined model. However, our structure of the HincII−DNA−Ca^{2+} complex shows increased order, albeit with relatively high (70−130 $Å^2$) temperature factors, in this region. Figure 3a shows a simulated annealing omit map of the linker of subunit A. The conformation of the linker of each subunit in the final refined model takes on slightly different conformations (Figure 3b). The segment lies in the minor groove of the bound DNA, making a hydrogen bond between the His 31 side chain and the guanine of the center step (underlined in GTCGAC) base pair (Figure 3c). The nature of this hydrogen bond is variable, however, with the His 31 side chain appearing to adopt different rotamer conformations as implied from its potential to hydrogen bond to either N2 of the center step guanine (underlined in GTCGAC) or O2 of the center step cytosine (underlined in GTCGAC, Figure 3c). The variable nature of the His 31−DNA interaction and of the linker region conformation in general (Figure 3b) may be important in accepting each of the three possible center step sequences recognized by HincII.

New DNA End Interaction. The DNA used in the cocrystallization is a 13-nucleotide oligonucleotide which is self-complementary and forms a duplex of 12 bp with a 5′ overhanging guanine. The oligonucleotides stack end to end throughout the crystal. The electron density of the 5′ nucleotide was not visible in the original structure, and the ends of each were originally modeled as blunt ended (Figure 4a, top). However, in the current structure it became clear that the 5′ guanine actually invades the neighboring duplex, kicking out the 3′ guanine, and hydrogen bonding with the second nucleotide of the oligonucleotide, which is a cytosine (Figure 4b, bottom). These interactions are positioned at crystallographic two-folds (as well as between the two independent dimers of the asymmetric unit), and the resulting interaction involves the base pairing between two nucleotides of each neighboring duplex. The ousted 3′ guanine stacks onto a tyrosine side chain of a HincII subunit which binds its parent duplex (Figure 4c). The simulated annealing omit map (Figure 4b) clearly shows that the DNA is not continuous from the invading 5′ guanine (Gua 1′) to the neighboring duplex (Gua 12). The observed interaction of the 5′ overhanging guanine with a neighboring duplex may explain the failure of oligonucleotides lacking this nucleotide to form isomorphous crystals (*40*). The original structure of the HincII−DNA complex has been refined with these DNA ends, lowering the R_{factor} from 21.9 to 20.4% and R_{free} from 28.4 to 27.1% (Table 1).

Active Site Arrangement. A single calcium ion was located and refined in each of the four crystallographically independent subunits of the asymmetric unit with final temperature factors of 21, 36, 48, and 45 $Å^2$ in subunits A−D, respectively. (The two other calcium ions modeled in the structure are bound to flanking DNA.) This position is well conserved in each subunit, with a root-mean-square deviation of 0.17 Å using the α-carbons of active site residues Asp 114, Asp 127, and Lys 129 for the superposition. An $F_o - F_c$ map after simulated annealing of the model with the calcium ion and all atoms within a 5 Å radius omitted is shown in Figure 5a. The calcium ion is ligated to two solvent molecules modeled as water, the backbone carbonyl of Val 128, one carboxylate oxygen each from Asp 114 and Asp 127, and the scissile phosphate *pro*-S_p oxygen (Figure 5b) in an octahedral arrangement with calcium ion−ligand distances varying from 2.0 to 2.5 Å. One of the ligated water

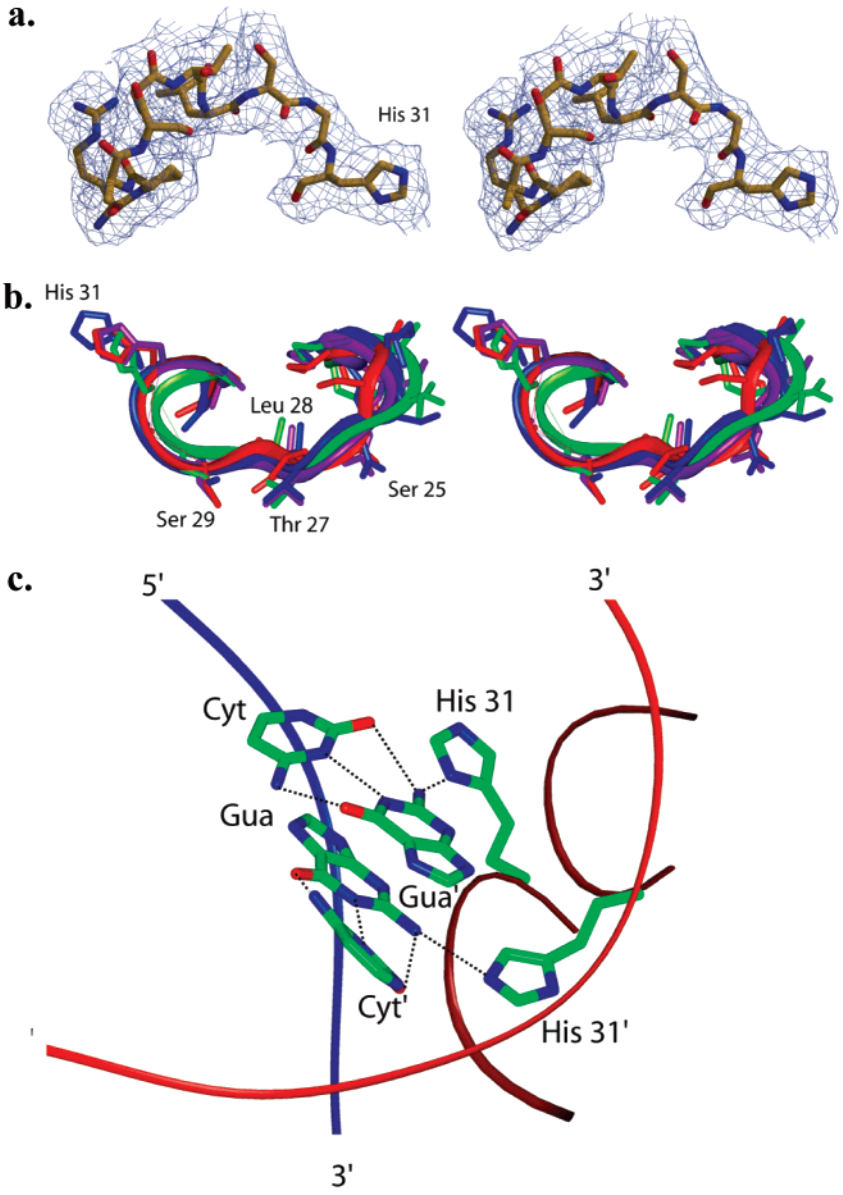

FIGURE 3: (a) Stereoview of the simulated annealing omit maps of residues 22−33 of subunit A with $F_o - F_c$ contoured at 3σ. (b) Stereoview of the superposition of residues 22−33 from each crystallographically independent subunits. Ribbons depict the path of the backbone, and selected side chains are shown. (c) Interaction of His 31 from subunits A and B in the minor groove of DNA. The DNA and protein backbones are shown as ribbons. Only the atoms of the bases of the two center base pairs and the side chains of His 31 from the two subunits are shown.

molecules (dark blue contour in Figure 4a and the upper apex as shown in Figure 5b) is well positioned to act as a nucleophile in the phosphodiesterase reaction, as it is within 2.7−3.2 Å of the scissile phosphate, and in-line with the O3′ leaving group (water−P−O3′ angles of 163−172°).

The arrangement of groups in the active site of subunit A is shown in Figure 5c. In addition to the Ca^{2+} ion, a second solvent molecule was found with ligation geometry and distances more typical of a metal ion than of water. This solvent molecule has been modeled as a sodium ion, and is in the position identical to that found in the original HincII−DNA cocrystal structure. It is ligated to the *pro*-R_p oxygen of the scissile phosphate as well as two water molecules, a backbone carbonyl oxygen, and one carboxylate oxygen of Asp 127 (Figure 5d). A sixth possible ligand is the nitrogen of active site Lys 129, although this distance is generally too long (2.7−4.1 Å) for inner sphere ligation. (A survey of 111 sodium ion−nitrogen bond lengths in the Cambridge Crystallographic Data Base resulted in a mean distance of 2.47 Å.)

Of interest to the discussion of the catalytic mechanism are the interactions around the attacking water and Lys 129. While this water molecule is well positioned to act as a nucleophile in subunits A and B, its distance from the calcium ion in subunit C is too long for inner sphere ligation (3.3 Å), and it is absent altogether from subunit D. Therefore, the interactions around this water and lysine are discussed for subunits A and B only. The attacking water is within hydrogen bonding distance of eight potential hydrogen bond donors or acceptors. However, the water molecule may only make four hydrogen bonding interactions at one time. The proximity of the water molecule to the carbonyl oxygen of Ile 128 and the carboxylate oxygen of Asp 127 is a consequence of its common ligation to the calcium ion with

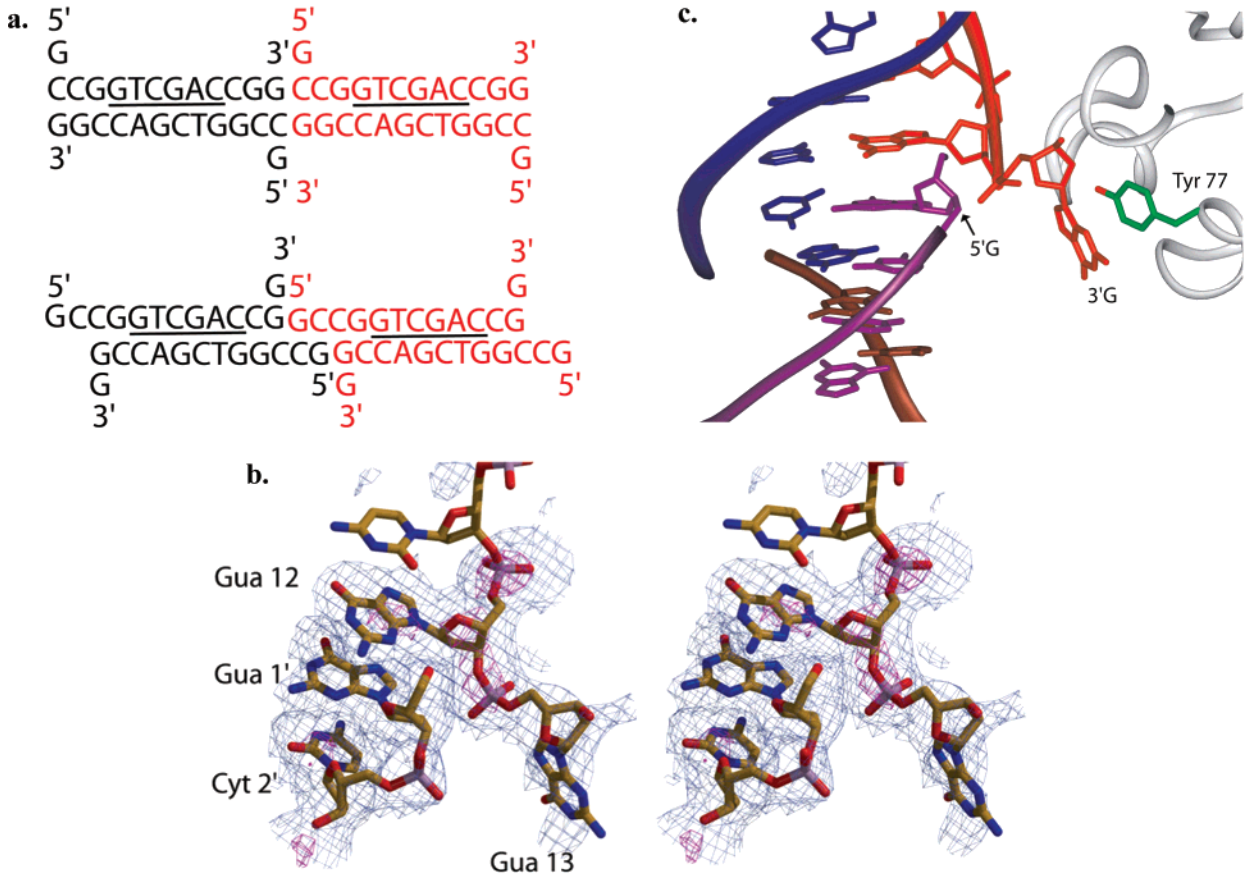

FIGURE 4: (a) DNA sequence at end-to-end stacking interactions. Separate duplexes are colored red and blackL (top) as modeled in the original HincII−DNA cocrystal structure and (bottom) revised model described here. (b) Simulated annealing omit maps of DNA ends with $F_o - F_c$ contoured at 3σ (blue) and 12σ (magenta), and $2F_o - F_c$ contoured at 1σ (gray). (c) Model of DNA ends. The continuous DNA backbone is shown as a ribbon, and atoms of the sugar phosphate backbone of selected nucleotides have been omitted for clarity. Blue and red represent DNA from one duplex, and purple and brown represent DNA strands from a neighboring duplex.

Table 1: Diffraction Data and Structure Refinement Statistics

	HincII−DNA−Ca^{2+}	HincII−DNA
cell dimensions	$a = 67.0$ Å, $b = 177.2$ Å, $c = 255.0$ Å, $\alpha = \beta = \gamma = 90°$	$a = 66.9$ Å, $b = 176.7$ Å, $c = 256.0$ Å, $\alpha = \beta = \gamma = 90°$
resolution (Å)	2.8	2.5
total no. of observations	112414	96955
no. of unique observations	36795	45516
% complete	96.9	86.6
I/σ	5.3	16.6
multiplicity	2.7	2.1
R_{sym}[a] (%)	6.6	4.7
R_{cryst}[b] (%)	18.0	20.4
R_{free}[c] (%)	28.6	27.1
overall B factor (Å^2)	55.1	56.5
rmsd for bond lengths (Å)	0.008	0.006
rmsd for bond angles (deg)	1.14	1.13
no. of waters	765	776
no. of metal ions	4 Na^+, 6 Ca^{2+}	2 Na^+

[a] $R_{sym} = \sum_{hkl}|\langle I_{hkl}\rangle - I_{hkl}|/\sum_{hkl} I_{hkl}$, where $\langle I_{hkl}\rangle$ is the average intensity over symmetry-related reflections and I_{hkl} is the observed intensity for reflection *hkl*. [b] $R_{cryst} = \sum_{hkl}||F_o| - |F_c||/\sum_{hkl}|F_{obs}|$, where F_o and F_c are the observed and calculated structure factor amplitudes, respectively, for reflection *hkl*. The sum is carried out over 95% of the observed reflections which are used in refinement. [c] R_{free} refers to the R factor for the test reflection set (5% of the total observed reflections) which was excluded from refinement.

these atoms. This, and the fact that these groups are in a poor arrangement to hydrogen bond to the water, and that their potential as hydrogen bond partners may be weakened due to their ligation to calcium ion, decreases their likelihood of being real hydrogen bonding partners with the nucleophile. Close distances of the water molecule to the *pro*-R_p or *pro*-S_p oxygen of the scissile phosphate may be a result of hydrogen bonding interactions as well, or merely a consequence of the placement of the water for nucleophilic attack on the phosphorus atom. The hydrogen bond distance between the side chain nitrogen of Lys 129 and the nucleophile is typically long, 3.3 Å, suggesting a weak interaction, although the coordinate error in this structure is 0.30 Å. Finally, the distances between the water and the *pro*-R_p oxygen of the phosphate 3′ to the scissile phosphate (2.6−3.0 Å) are consistent with a good hydrogen bond between these groups.

The geometry around active site Lys 129 is similarly crowded with potential hydrogen bonding partners, including the attacking water, a carboxylate oxygen of Asp 127, the backbone carbonyl of Asn 141, the *pro*-R_p oxygen of the scissile phosphate, and the sodium ion. The distance between the lysine side chain nitrogen and the sodium ion is relatively long, as mentioned above, suggestive of the lack of an inner sphere ligation; however, an effect on the pK_a of the nitrogen could be expected by the proximity of a positive charge.

Binding Measurements for HincII to DNA Substrates. To test the effect of removing the phosphate 3′ from the scissile phosphate on the DNA binding affinity of HincII, gel shift measurements were performed. The measured apparent dissociation constants, K_D, of HincII and the various DNA

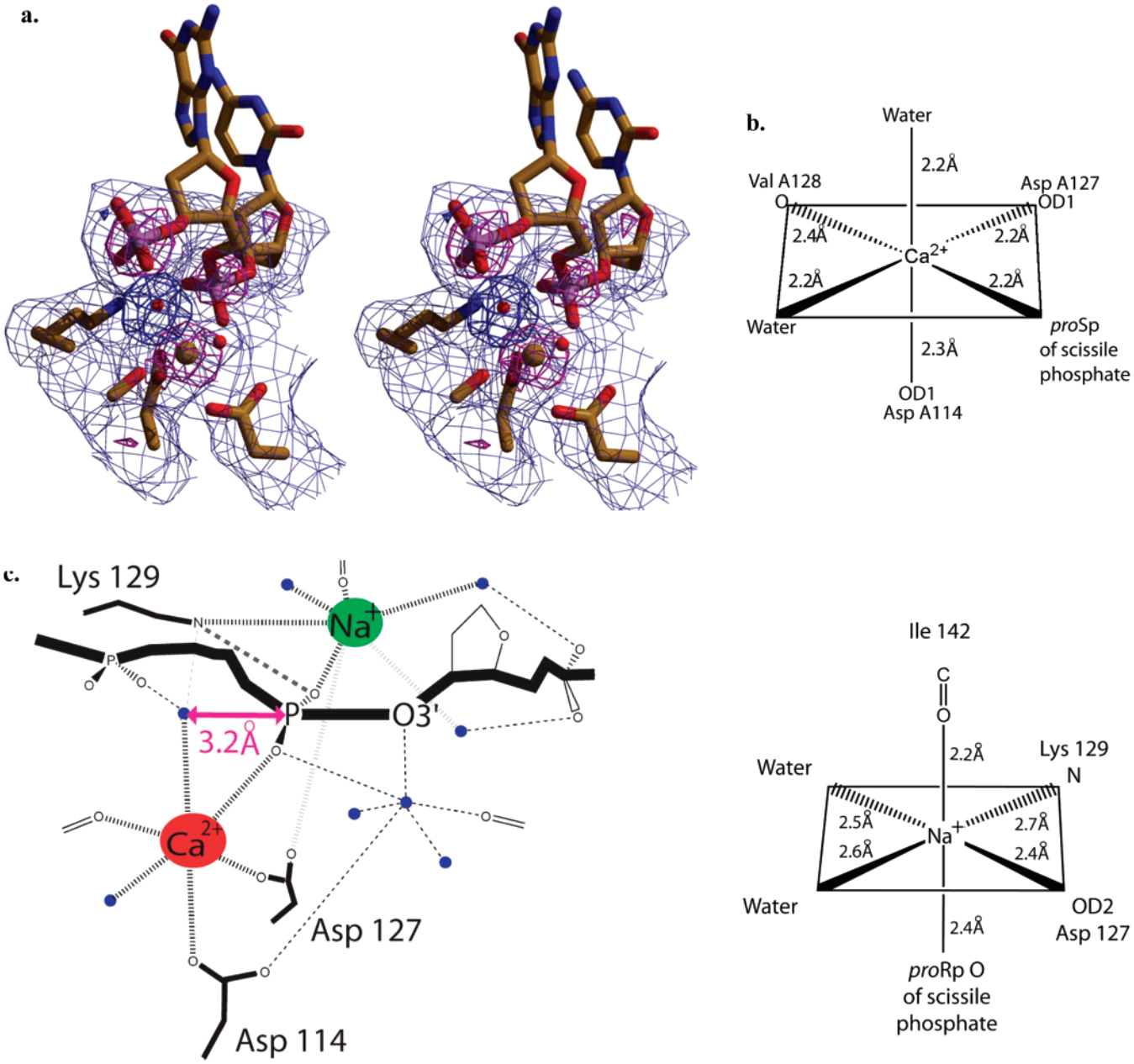

FIGURE 5: (a) Stereoview of the simulated annealing omit maps and atoms of the active site of subunit A. Water molecules are shown as red spheres. Atoms within 5 Å of and including the calcium ion (yellow sphere) were omitted prior to simulated annealing and calculation of an $F_o - F_c$ map contoured at 3σ (light blue) and 12σ (pink) for this region only. A separate simulated annealing and $F_o - F_c$ map calculation was performed with the attacking water omitted and contoured at 3σ (dark blue). (b) Geometry and bond lengths around the calcium ion of active sites in subunit A. Although the structure was drawn with perfect octahedral symmetry, deviations in bond angles exist. (c) Schematic diagrams of the interactions in the active site of subunit A with the calcium ion shown as a red ellipsoid, the sodium ion as a green ellipsoid, and water molecules as blue circles. Ligations to metal ions are shown as thicker dashed lines when distances between appropriate groups were between 2.2 and 2.5 Å. Hydrogen bonds are shown as dashed lines when distances between appropriate groups were between 2.4 and 3.3 Å. (d) Geometry around the sodium ion of active site A. Although the structure was drawn with perfect octahedral symmetry, deviations in bond angles exist.

substrates are shown in Table 2. A representative gel shift autoradiogram is shown in Figure 1b, and the corresponding fit of the data in Figure 1c. HincII binds to the 16mer and 32mer duplex DNA oligonucleotides with apparent dissociation constants of approximately 1.1 ± 0.23 and 0.53 ± 0.17 nM, respectively, in the presence of 5 mM $CaCl_2$. The 32mer duplex substrates containing one disrupted strand, missing the phosphate 3′ to the scissile phosphate, have apparent K_D values with HincII of 1.9 ± 1.2 and 1.6 ± 1.7 nM, respectively. Therefore, the absence of the phosphate 3′ to the scissile phosphate, in the context of the 32mer duplex DNA, may result in weakened binding; however, this weakening is not more than 10-fold.

Single-Turnover Cleavage Rate Constant Measurements for HincII and DNA Substrates. To assess the importance of the observed Na^+, as well as the phosphate 3′ to the scissile phosphate, to the HincII cleavage mechanism, single-turnover cleavage rate constants (k_{cleave}) of HincII with the DNA substrates either in the absence of Na^+ or with substrates missing the phosphate 3′ to the scissile phosphate were measured (Table 3). These rates are measured in the presence of excess HincII enzyme over DNA substrate, and

Table 2: Apparent Dissociation Constants of HincII and DNA Substrates[a]

DNA substrate	K_D (nM)	standard deviation (nM)
16mer	1.14	0.23
32mer intact	0.53	0.17
32mer missing 3′-P on the top strand[b]	1.9	1.2
32mer missing 3′-P on the bottom strand	1.6	1.7

[a] Binding conditions: 37 °C in 50 mM Bis-Tris propane (pH 7.5), 5 mM $CaCl_2$, 1 mM DTT, 0.1 mg/mL BSA, and NaCl to the conductivity of a reference solution containing 50 mM Bis-Tris propane (pH 7.5), 140 mM NaCl, 1 mM DTT, and 0.1 mg/mL BSA. [b] Average of only two measurements.

at concentrations where more than 99% of the substrate DNA should be bound to the HincII enzyme. A representative scan of the HEX-bound DNA from reaction incubations is shown in Figure 1d, and the fit of the data to determine k_{cleave} in Figure 1e. The k_{cleave} values of HincII for the intact 16mer duplex oligonucleotides in the presence of NaCl are 6.6×10^{-2} and 4.9×10^{-2} s^{-1} for the top and bottom strands, respectively. These rate constants are slower relative to those of related endonucleases [that of EcoRV is 0.3 s^{-1} (*23*)]; however, the single-turnover rate constants of HincII and the 16mer HEX substrate are increased 5-fold when initiation of the reaction occurs by adding Mg^{2+} to the premixed HincII/DNA solution. Thus, the single-turnover rate constants described herein, although modeled very well to a single exponential, likely include contributions from steps occurring prior to cleavage, including binding and/or duplex intercalation.

Using NH_4Cl in place of NaCl results in a k_{cleave} values of 9.0×10^{-2} and 8.0×10^{-2} s^{-1} for the top and bottom strands, respectively. Thus, the presence of Na^+ in the reaction buffer appears to decrease the single-turnover rate constant of cleavage by 1.6−1.4-fold.

Using the NaCl reaction buffer, the single-turnover cleavage rate constants of HincII and the 32mer substrate are 9.0×10^{-3} and 2.8×10^{-2} s^{-1} for the top and bottom strands, respectively. These rate constants are 2−5-fold decreased relative to that of the 16mer substrate. As indicated above, the single-turnover cleavage rates likely measure events prior to, and in addition to, DNA cleavage. These events include DNA binding and duplex intercalation, and the longer substrates may result in a decrease in the rates of these steps, rather than the actual rate of DNA cleavage itself.

When substrates are composed of one continuous 32mer strand, and one discontinuous strand, missing a phosphate 3′ from the scissile phosphate, the single-turnover cleavage rates are altered. No cleavage of the disrupted strand is seen even after 17 h, although the enzyme remains active after this time (data not shown). Assuming that no more than 10% cleavage (a generous lower limit of detection) has occurred in this time, an upper limit on the single-turnover rate of cleavage can then be estimated to be 1.7×10^{-6} s^{-1}. The continuous strand, present as either the top or bottom in a disrupted substrate, is cleaved by HincII, however, at a greatly reduced rate (10−100-fold).

DISCUSSION

Catalytic Mechanistic Models of Related Endonucleases. The three-dimensional crystal structures of more than 10 type II restriction endonucleases have been determined, and in seven cases, the positions of particular divalent cations in the enzyme−substrate and/or enzyme−product complexes have been determined. The positions of these cations provide insight into the roles of these ions in the catalysis of the DNA phosphodiester backbone cleavage reaction. Currently, variability exists in the roles of active site groups, including the divalent cations, among the DNA cleavage mechanisms proposed for type II restriction endonucleases. This may arise in part from the use of different enzymes in these studies; the catalytic mechanism, and in particular the roles of each of these groups, may not necessarily be conserved. However, even within the same enzyme, EcoRV, at least four distinct mechanisms have been proposed (*15*, *22*, *25*, *30*). These mechanisms have been proposed on the basis of not only crystal structures but also biochemical investigations, such as the requirement for the 3′ phosphate (*30*), and stopped flow kinetic studies (*25*). The biochemical and kinetic studies provide valuable information, but limited atomic detail. On the other hand, the crystal structures suffer from the difficulty in trapping an active ground state complex prior to cleavage. Product complexes show the positions of atoms after the reaction, but prereaction complexes must be stalled prior to cleavage to complete the structural analysis. Since structural analysis generally takes several days, from the time the crystals are prepared to data collection, only relatively inactive complexes can be studied. This fact leaves open the possibility that the observed complexes are "off pathway", or in a nonproductive and irrelevant dead end. However, analysis of many such complexes can increase confidence in a model for the catalytic mechanism that is consistent with the observed structures, as well as the nature of their inhibition.

The hydrolysis of the DNA backbone by type II restriction endonucleases involves an in-line attack of water, or hydroxide, on the scissile phosphate, resulting in a pentacovalent trigonal bipyramidal transition state which collapses with inversion of configuration and release of the 3′ oxygen (*52*−*54*). The reaction is in-line with the nucleophile and 3′ oxygen leaving group occupying axial positions of the trigonal bipyramidal transition state (Figure 6a). An enzyme is believed to be capable of accelerating this reaction by a number of means, including orienting active site groups, facilitating nucleophilic attack through activation of the nucleophile, stabilizing the additional negative charge which forms on the transition state, and stabilizing the 3′ oxygen leaving group (*55*). The divalent cations, or metal ions, bound in the active sites of these enzymes are believed to be critical in some, or all, of these roles. The now "classical" two-metal ion mechanism was originally proposed by Steitz and coworkers (*21*) in their studies of the exonuclease reaction catalyzed by the Klenow fragment of *E. coli* DNase I. This mechanism involves the placement of the two metals along a line that is parallel to the would-be axis of the trigonal bipyramidal transition state. The metal ion at site A is in an optimal position to activate the nucleophile by ligation and lowering its pK_a to produce hydroxide, and to stabilize the transition state by direct ligation to a nonesterified oxygen of the scissile phosphate. The metal ion at site B is also positioned to stabilize the transition state by ligation to the scissile phosphate, and importantly also to stabilize the leaving group through direct ligation. Both metal ions may

Table 3: Single-Turnover Rate Constants[a]

DNA substrate and buffer	k (s^{-1})	standard deviation (s^{-1})
16mer with NaCl		
top strand	6.6×10^{-2}	0.8×10^{-2}
bottom strand	4.9×10^{-2}	1.4×10^{-2}
16mer with NH_4Cl		
top strand	9.0×10^{-2}	0.9×10^{-2}
bottom strand	8.0×10^{-2}	0.3×10^{-2}
32mer intact		
top strand	9.0×10^{-3}	0.6×10^{-3}
bottom strand	2.8×10^{-2}	0.4×10^{-2}
32mer missing 3′-P on the top strand		
top (discontinuous) strand	$<1.7 \times 10^{-6}$ (no cutting after 17 h)	–
bottom (continuous) strand	2.0×10^{-3}	0.3×10^{-3}
32mer missing 3′-P on the bottom strand		
top (continuous) strand	9.7×10^{-5}	0.6×10^{-5}
bottom (discontinuous) strand	$<1.1 \times 10^{-6}$ (no cutting after 27.5 h)	–

[a] Reaction conditions: 37 °C in 50 mM Bis-Tris propane (pH 7.5), 10 mM $MgCl_2$, 1 mM DTT, 0.1 mg/mL BSA, and NaCl to the conductivity of a reference solution containing 50 mM Bis-Tris propane (pH 7.5), 140 mM NaCl, 1 mM DTT, and 0.1 mg/mL BSA.

serve to organize and orient the active site groups. All metal ion-dependent phosphoryl transfer mechanisms subsequently proposed for enzymes utilize some, or all, of these features. Differences in the various proposed mechanisms include the substitution of a positively charged side chain for one of the metal ions, whether both metal ions ligate the scissile phosphate, and whether metal ion B directly ligates the leaving group, or alternatively stabilizes it by activating a metal-ligated water to protonate the leaving group. Another important point of discussion regarding the different mechanisms is the need for, and identity of, a general base to accept the proton from the attacking water.

Studies on type II restriction endonuclease EcoRV are the most comprehensive structural studies of divalent cation binding to an enzyme in this class (*15*, *22*, *56*−*58*). This analysis has resulted in a mechanism involving three metal ion positions (*15*), shown in Figure 6b, which has two sites, sites I and III, in common with sites A and B of the classical two-metal ion mechanism. However, the position of site III is closer to site I than in the two-metal ion mechanism, and is not directly ligated to the O3′ leaving group. The third metal ion of the EcoRV mechanism, that in site II, has been observed in many of the structures; however, its role in the cleavage reaction originally appeared to be indirect. Recently, new evidence suggests a more direct role in catalysis (*58*). Although, or perhaps because, this enzyme has been so well studied by several research groups, its mechanism has remained the most controversial.

Evidence suggests that EcoRV and HincII evolved from a common ancestor (*32*, *59*), despite the fact that these two enzymes have levels of sequence identity (9%) well below that which indicates homology (*60*). The similar DNA target sequence, pattern of cutting (they both cut DNA to leave blunt ends), and especially the presence of the same folding topology argue for an evolutionary relationship between these two enzymes. Given the common fold and function of the structurally characterized type II enzymes, they are all likely to have a common ancestor; however, HincII and EcoRV are likely to be more recently diverged. It is therefore of interest to closely compare the mechanistic features of these two enzymes. Similarly, it would be expected that all blunt cutting enzymes should be more similar in mechanism to each other than to sticky cutting enzymes.

Restriction endonucleases have been known to possess a conserved $PDX_n(D/E)XK$ motif (*26*). The two acidic residues appear to be responsible for ligating the divalent cations, and at least one, if not both, has been consistently proposed to do so in all reported mechanistic models. The role of the lysine residue is less clear, although in cases tested it is extremely important to catalysis (*61*, *62*). However, it is not strictly conserved, and has been observed as a glutamate in BamHI, and a glutamine in BglII. In some models, i.e., that of PvuII (*16*), EcoRV (*15*), and BglI (*20*), the lysine is protonated, and is purported to stabilize the additional negative charge which forms on the transition state. Clearly, the glutamate of BamHI cannot perform this same function. However, both lysine and glutamate may act as general base catalysts if their respective pK_a values have been modulated to that near the enzyme's optimal pH. Such modulation has been known to occur for residues buried within proteins. The mechanistic model proposed for BamHI does utilize the glutamate as a general base (*17*). A complication in the generality of the role of this residue in restriction endonucleases was the discovery of a glutamine in this position in the structure of BglII (*18*). However, the third general role proposed for this residue is to orient the nucleophile, and clearly, the glutamine is capable of only this role. This example illustrates the potential problem with making generalizations with respect to the roles of the active site residues as they may not be conserved in each enzyme. Mutagenic studies on only selected enzymes have been used to generalize their roles to all enzymes. Mutagenic and biochemical studies need to be performed on each structurally characterized enzyme to determine the conservation of roles and importance of each group to the catalytic reaction.

Other differences in two-metal ion mechanisms proposed to date include the ligations of the scissile phosphate, as well as the leaving group, by the metal ions. Direct ligation to the leaving group by metal ion B of the two-metal ion mechanism is implicated in BglI and BamHI. No direct ligation is implicated in NgoMIV, EcoRV, or PvuII; instead, the mechanism involves protonation of the leaving group by a metal-ligated water. Direct ligation to the *pro*-S_p oxygen of the scissile phosphate by both metal ions is implicated in the mechanisms of PvuII, BglI, BamHI, and NgoMIV. Of the mechanisms implicating more than one metal ion, only

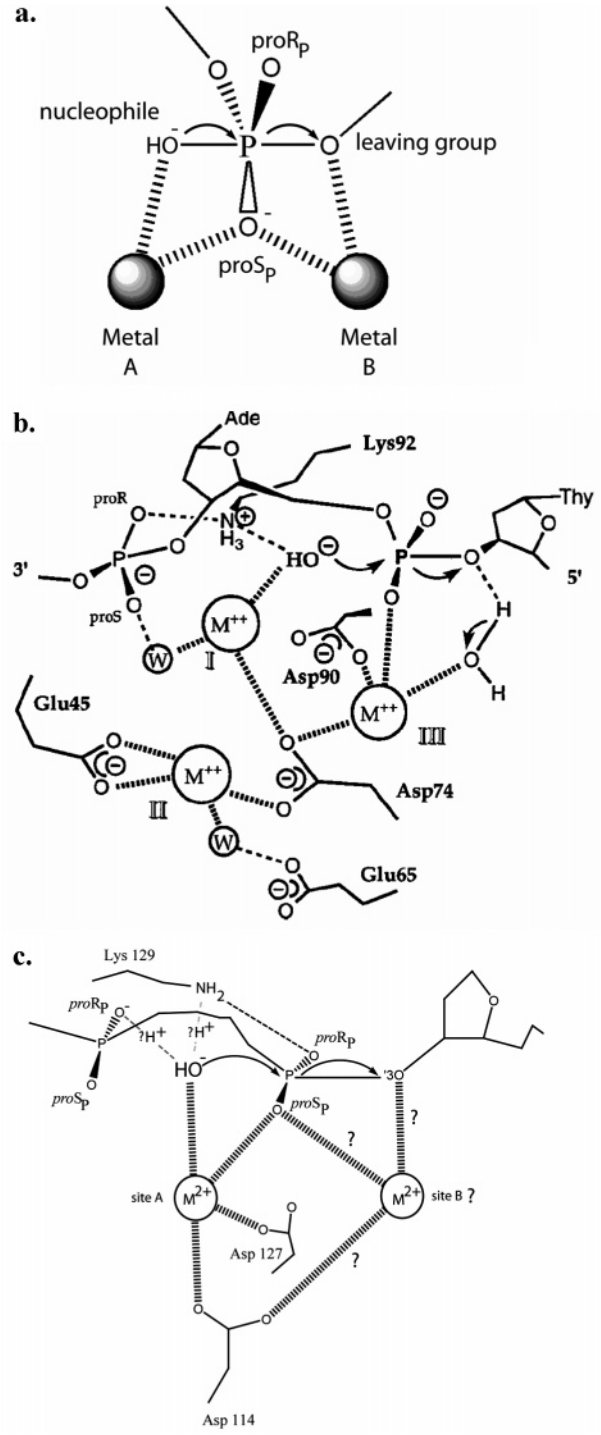

FIGURE 6: (a) Two-metal ion mechanim with metal ions shown as gray spheres. (b) Three-metal ion mechanism of EcoRV (*15*) (Copyright 1998 National Academy of Sciences). (c) HincII mechanism. Question marks around the site B metal ion and the proton abstraction by Lys 129 or the 3′ phosphate indicate interactions that may be possible but require additional investigation.

that proposed for EcoRV does not include direct ligation of the *pro-S*$_p$ phosphodiester oxygen by both ions. The ion without direct ligation is that in site I of the three-metal ion mechanism (Figure 6b), analogous to site A of the two-metal ion mechanism. This inconsistency of the three-metal mechanism with other type II mechanistic models could be a consequence of the use of multiple structures to derive it, since all three metal ion sites are not observed in the same structure. Further, the DNA in the structure containing a site

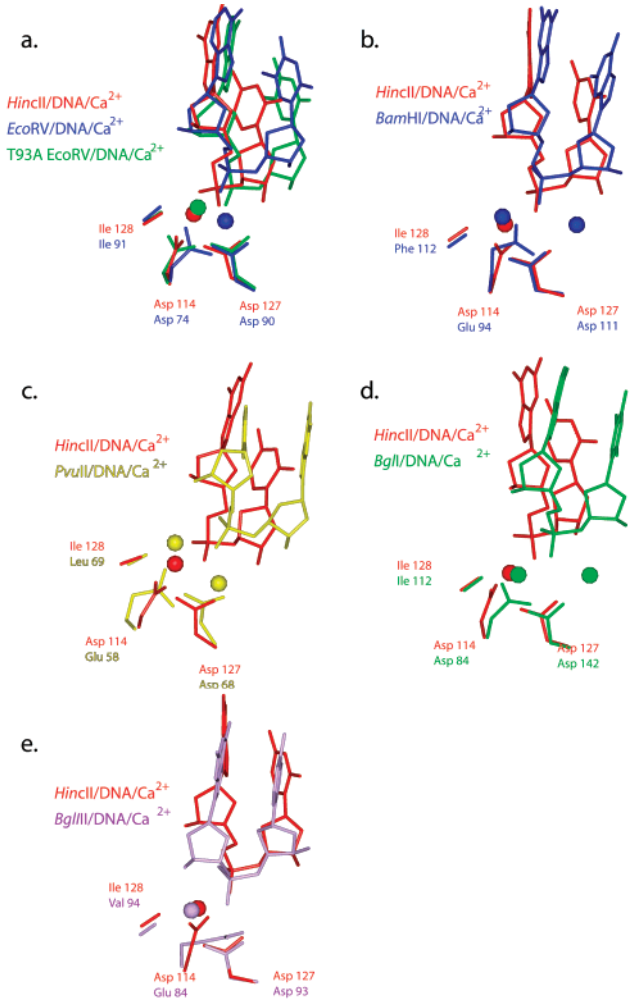

FIGURE 7: Superposition of *Hinc*II−DNA−Ca^{2+} active site A (red) with (a) EcoRV bound to cognate DNA and cocrystallized with Ca^{2+} (blue) and T93A EcoRV bound to cognate DNA and cocrystallized with Ca^{2+} (green), (b) BamHI bound to cognate DNA and cocrystallized with Ca^{2+} (blue), (c) PvuII bound to cognate DNA and soaked in Ca^{2+} (yellow), (d) BglI bound to cognate DNA and Ca^{2+} (green), and (e) BglII bound to cognate DNA and Ca^{2+} (purple).

I ion is shifted, due to a mutation in the protein, away from the active site, and thus, direct ligation is not possible.

Binding of Ca^{2+} to HincII. The cocrystal structure of HincII with cognate DNA soaked in 50 mM $CaCl_2$ shows the Ca^{2+} ion in the position labeled site I in the three-metal ion mechanism (Figure 6b), or site A in the two-metal ion mechanism (Figure 6a). Panels a−e of Figure 7 show that the position of this ion overlaps very closely with these sites in EcoRV, PvuII, BamHI, BglII, and BglI. The role of this ion in the various mechanistic models has been proposed to be the activation of the attacking water, by lowering its pK_a, and enhancing its deprotonation. In some cases, its role has also been suggested to be the stabilization of the additional charge which forms on the transition state, as a result of nucleophilic attack by a hydroxide ion, through ligation to the *pro-S*$_p$ oxygen of the scissile phosphate. The site A metal ion here, in the HincII−DNA−Ca^{2+} structure, does ligate the *pro-S*$_p$ oxygen, as well as a water in a good position for nucleophilic attack. The ligation to the scissile phosphate is variable in the other two blunt cutters, being present in PvuII, but absent in EcoRV. Therefore, heterogeneity, or divergence, may exist among the blunt cutting type II restriction

endonucleases with respect to the site I metal ion. Alternatively, the lack of direct ligation of this metal ion to the scissile phosphate in EcoRV may be an artifact of the structural studies (see above). The direct ligation by this metal ion does also exist in all mechanisms proposed to date for 5′ and 3′ sticky cutting enzymes, including BamHI, NgoMIV, BglII, and BglI.

Only a single Ca^{2+} ion is found in each active site, at site A, although the two-metal ion mechanism predicts a second, at site B (Figure 6a). Indeed, studies of binding of Mn^{2+} to *Hinc*II indicate occupation of both sites A and B predicted by the two-metal ion mechanism (C. Etzkorn and N. C. Horton, unpublished results). The crystallization, soaking, and cryoprotectant experiments are all performed at pH 5.5. Although the pH optimum of HincII is not known, the optimum for EcoRV is approximately pH 8.75 (*23*), and no cutting is detectable at pH 5.5. Preliminary data with HincII do indicate that some amount of cleavage occurs at pH 5.5 (C. Etzkorn and N. C. Horton, unpublished results). It is possible that the site B Ca^{2+} position may become occupied at more optimal pHs. However, the ligation of the site B divalent cation is expected to include one or both of the active site aspartates, Asp 114 and Asp 127, which are already both involved in ligation to the first divalent cation, and Asp 127 is ligated to the sodium ion. It is difficult to see how either of these two residues may be protonated at pH 5.5 given their ligation to mono- and divalent cations. Perhaps ligation to the sodium ion is preventing binding of the second divalent cation; however, how increasing the pH would disrupt the sodium ion binding is unclear. In addition, single-turnover cleavage rate measurements show only very slight inhibition of the reaction in the presence of Na^+ relative to that with NH_4^+ (and Na^+ free) containing buffer. Interestingly, the BglII structure was determined at pH 5.2, and only a single Ca^{2+} is seen in site A. Given the information described herein with Ca^{2+}, we cannot say whether site B would be occupied by Mg^{2+}. Therefore, the mechanistic model for HincII shown in Figure 6c shows a site B metal ion; however, there are question marks on it and its interactions to indicate that they cannot be predicted from the Ca^{2+}-bound structure.

Why Does Ca^{2+} Inhibit DNA Cleavage by HincII? The fact that increasing concentrations of calcium ion can inhibit Mg^{2+}-catalyzed DNA cleavage by restriction endonucleases has been attributed to the competition of Ca^{2+} for at least some of the Mg^{2+} binding sites (*63*). This prediction has been borne out by structural studies which show Ca^{2+} binding in the active site of restriction endonucleases at the scissile phosphate. However, the structural or chemical means by which this inhibition results are not precisely known. The Ca^{2+} ion (0.99 Å) is larger than Mg^{2+} (0.80 Å), and Ca^{2+} allows more than six ligands with less geometric stringency than Mg^{2+} (*64*, *65*). The inhibition of cleavage in the presence of Ca^{2+}, despite the fact that Ca^{2+} binds in the active site, is generally attributed to slight mispositioning of active site groups as a result of its different size and geometry. In addition, the pK_a of a water molecule ligated to Ca^{2+} (12.8) is much higher than that ligated to Mg^{2+} (11.4) (*66*), although this does not seem to be wholly responsible for inhibition since reactivity cannot be restored by increasing the pH. As mentioned above, the two-metal ion mechanism predicts a second divalent cation binding to the active site, and therefore, its absence should inhibit cleavage. However, two Ca^{2+} ions have been observed in the active sites of several other restriction endonucleases, which remained inhibited.

Finally, it has been suggested that, in the case of the phosphodiesterase activity of *E. coli* ribonuclease H1 (*67*), Ca^{2+} inhibits catalysis by ligating an aspartate residue that is free in the Mg^{2+}-catalyzed reaction, which performs general base catalysis. If this mechanism of inhibition were operative in the restriction endonucleases, the best candidate for the residue that is involved would be the second acidic residue of the motif, or Asp 127 in HincII. The homologous residue in other restriction endonuclease structures does show variation in its ligation to the site A metal ion, depending on whether the site is occupied by Ca^{2+} or a divalent cation that confers activity, Mg^{2+} or Mn^{2+}. This residue of PvuII, BglI, BamHI, and EcoRV, but not BglII, is ligated to the site A ion when occupied by Ca^{2+}. The only Mn^{2+}- or Mg^{2+}-containing structures are those of BamHI, NgoMIV, and EcoRV, with only product structures (with cleaved DNA) reported for BamHI (*17*) and NgoMIV (*19*), but structures showing both cleaved and uncleaved DNA with Mg^{2+} are available for EcoRV (*22*, *56*, *58*). NgoMIV possesses a serine at the position of Asp 127, but an acetate molecule is observed in the structure of NgoMIV with cleaved DNA, apparently taking on the role of the usual aspartate/glutamate by ligating the two Mg^{2+} ions found in the active site. However, the Asp 127 homologue in BamHI and EcoRV is not ligated to the divalent cation (Mn^{2+} or Mg^{2+}) in the product structures. Interestingly, the Asp 127 homologue (Asp 90) is ligated to Mg^{2+} in two stalled complexes of EcoRV, that of wild-type EcoRV bound to DNA soaked in Mg^{2+} (*22*) and a mutant with the active site lysine mutated to alanine, bound to DNA and cocrystallized with Mg^{2+} (*58*). Thus, the difference in ligation of the divalent cation by the Asp 127 homologue could be a mechanism of inhibition by Ca^{2+}; alternatively, the ligation of the metal ion to the Asp 127 homologue may change as the reaction proceeds from uncleaved to cleaved DNA.

Importance of the Phosphate 3′ to the Scissile Phosphate. The report that a substrate lacking the phosphate 3′ of the scissile phosphate (*30*) could not be cleaved by EcoRV led to the proposal that this phosphate activates the attacking water by general base catalysis. Weaknesses of this proposal are the low pK_a of the phosphate oxygens (1.5−1.7) and the high pH optimum of enzyme activity (pH 8.75 for EcoRV). A subsequent interpretation of the importance of this phosphate is related to its involvement in stabilizing the site I (or site A) metal ion position in EcoRV (*15*). In the three-metal ion mechanism of EcoRV, the site I metal ion is ligated through a water molecule, different from the attacking water, to the *pro*-S_p oxygen of the 3′ phosphate (Figure 6b). In the case of HincII, the nucleophile is directly hydrogen bonded to the *pro*-R_p oxygen of the 3′ phosphate. Phosphorothioate modification studies of the 3′ phosphate of EcoRV substrates indicate that this enzyme can cleave a substrate substituted at the R_p position, but not the S_p position (*68*), suggesting that it is the *pro*-R_p oxygen of the 3′ phosphate acting as the proton acceptor. The hydrogen bond from the attacking water to this atom places it in a good position to act as a proton acceptor. It is also in a good position to stabilize the binding of Mg^{2+} to site A (through interaction with the attacking water), as well as to orient the attacking water. Unfortunately, the vast number of potential hydrogen bonding partners

precludes a proper hydrogen bond inventory of the attacking water molecule. However, intuitively it would appear to be very counterproductive to place a negatively charged group within hydrogen bonding distance of a water molecule that requires deprotonation for activation. It seems likely that the 3′ phosphate is either protonated or becoming protonated by the nucleophile.

Methyl phosphonate substitution of the 3′ phosphate in the substrates of a number of enzymes suggests its importance in substrate-assisted catalysis, including PvuII (*69*), and structural analysis shows that the would-be attacking water molecule is within hydrogen bonding distance of the *pro*-R_p oxygen of the 3′ phosphate in the PvuII structure bound to DNA and Ca^{2+} (*16*). The modification studies also showed that BglII was not inhibited by the substitution, and its attacking water is 4.3 Å from the *pro*-R_p oxygen, too far for hydrogen bonding. Thus, in these two cases, the presence, or absence, of a hydrogen bond between the attacking water and the 3′ phosphate correlates with the importance of that group to DNA cleavage.

Kinetic studies (Table 3) show that this group is also important to DNA cleavage by HincII, as it is in EcoRV. Though the single-turnover cleavage rates likely include some contributions from events prior to DNA cleavage such as binding (see above), Table 2 shows that the absence of the 3′ phosphate does not appear to appreciably weaken the binding of disrupted substrates to HincII. The single-turnover cleavage rate measurements show that HincII will not cleave the disrupted strand, missing this 3′ phosphate, in duplex DNA containing one continuous strand, even after 17 h, and that the HincII cleavage of the intact strand in such a duplex is weakened by 10−100-fold. This fact suggests that the absence of the 3′ phosphate on a DNA strand in one active site affects DNA cleavage within the other active site of the HincII dimer. Such an effect could occur if the HincII, and/or the DNA bound to HincII, modifies its conformation relative to HincII bound to fully intact DNA, to minimize the negative effect of the missing phosphate. This change in conformation could be propagated from the origin of the disruption, at the site of the missing 3′ phosphate, to the opposite active site within the HincII dimer. Such structural adaptation also minimizes negative effects on binding affinity in modified complexes (*70*). Therefore, the kinetic and binding data are consistent with a role of the 3′ phosphate either directly in catalysis or in the positioning of active site groups, within both its own active site and the opposite active site of the HincII dimer.

HincII Mechanistic Model. A schematic of the mechanism for DNA cleavage by HincII derived from this work is shown in Figure 6c. Although only a single Ca^{2+} ion, in site A, was found in the active sites of HincII bound to DNA described herein, two divalent cations are positioned as in the classical two-metal ion mechanism in Figure 6c. Question marks around the site B ion show the likely position and interactions this ion would make, following previous studies of phosphoryl transfer enzymes, and especially the two-metal ion mechanism. The functions of the ions in the mechanism are as follows: the ion at site A ligates the attacking water, lowering its pK_a, while the ion at site B directly ligates the leaving group. Both metal ions stabilize the incipient negative charge of the transition state through direct ligation to the *pro*-S_p oxygen of the scissile phosphate. They are each ligated by a single carboxylate oxygen of Asp 114 and Asp 127. The attacking water is hydrogen bonded to the *pro*-R_p oxygen of the neighboring 3′ phosphate, as well as the side chain of Lys 129.

The identity of the proton acceptor has not been determined from the current study; however, two active site moieties are in an appropriate position to perform this function. Both the active site lysine, Lys 129, and the *pro*-R_p oxygen of the 3′ phosphate are within hydrogen bonding distance of the attacking water. Kinetic studies of the importance of Lys 129 to the cleavage reaction by HincII have not been performed, but the homologous residue in other restriction endonucleases, such as EcoRV, indicate that mutation to alanine diminishes the activity by 10^4-fold (*62*). Kinetic studies performed here show that the 3′ phosphate is critical to DNA cleavage within its own DNA strand, but not to single disrupted duplex binding, by HincII. Though these studies show that these groups are important to catalysis, they do not disclose their means of action. Other functions, excluding general base catalysis, could be performed by these groups. Either could serve to orient the nucleophile, and the lysine, if protonated, could function to electrostatically stabilize the transition state. Orienting the nucleophile is the only function possible for all residues observed in the lysine position in type II restriction endonucleases, including glutamate and glutamine. On the other hand, the 3′ phosphate could serve to stabilize the site A metal ion, which is similar, although different in the details, to that proposed in the three-metal ion mechanism (Figure 6b) (*15*).

Although the pK_a of a phosphate group is very low (1.7), indicating that the group remains deprotonated until very high concentrations of protons are reached, its position hydrogen bonding to the attacking water suggests a possible role as the general base. The reason for this is that it would be very anticatalytic to place a negatively charged group next to the nucleophile, which is presumed to be activated by deprotonation to hydroxide. Therefore, it is likely either to be protonated or to become protonated by the nucleophile, before the reaction could occur. The shifting of the pK_a of the phosphate to perfom this function could be accomplished by its burial in the enzyme active site, although this is difficult to predict given the large number of titratable groups in its vicinity. Further studies are needed to elucidate the importance of this group to its possible functions, including stabilizing the site A metal ion and general base catalysis.

Concluding Comments. Many important features of the HincII catalytic mechanism have been found from the structure described herein, namely, the occupation of site A by a divalent cation, its direct ligation to the scissile phosphate, and ligation to a water well positioned to act as a nucleophile. However, many more details remain to be understood, including any additional divalent cation positions and their roles, and the roles of the 3′ phosphate and active site lysine, which will require additional investigations. These investigations, as well as those using related enzymes, will also address the issue of mechanistic divergence. Do these enzymes utilize different catalytic mechanisms, having different roles for the active site groups? If so, what are these roles? Only the combination of mutagenic, biochemical, computational, and structural studies of a number of phos-

phoryl transfer enzymes will answer these important questions.

ACKNOWLEDGMENT

Portions of this research were carried out at the Stanford Synchrotron Radiation Laboratory, a national user facility operated by Stanford University on behalf of the U.S. Department of Energy, Office of Basic Energy Sciences. The SSRL Structural Molecular Biology Program is supported by the Department of Energy, Office of Biological and Environmental Research, and by the National Institutes of Health, National Center for Research Resources, Biomedical Technology Program, and the National Institute of General Medical Sciences.

REFERENCES

1. Horton, N. C., and Perona, J. J. (2002) Making the most of metal ions, *Nat. Struct. Biol. 9*, 42−47.
2. Cowan, J. A. (1998) Metal Activation of Enzymes in Nucleic Acid Biochem, *Chem. Rev. 98*, 1067−1088.
3. Noble, C. G., and Maxwell, A. (2002) The role of GyrB in the DNA cleavage-religation reaction of DNA gyrase: a proposed two metal-ion mechanism, *J. Mol. Biol. 318*, 361−371.
4. Zhu, C. X., and Tse-Dinh, Y. C. (2000) The acidic triad conserved in type IA DNA topoisomerases is required for binding of Mg(II) and subsequent conformational change, *J. Biol. Chem. 275*, 5318−5322.
5. de Laat, W. L., Appeldoorn, E., Jaspers, N. G., and Hoeijmakers, J. H. (1998) DNA structural elements required for ERCC1-XPF endonuclease activity, *J. Biol. Chem. 273*, 7835−7842.
6. Ban, C., and Yang, W. (1998) Structural basis for MutH activation in E. coli mismatch repair and relationship of MutH to restriction endonucleases, *EMBO J. 17*, 1526−1534.
7. Kovall, R. A., and Matthews, B. W. (1998) Structural, functional, and evolutionary relationships between λ-exonuclease and the type II restriction endonucleases, *Nat. Struct. Biol. 95*, 7893−7897.
8. Tsutakawa, S. E., Muto, T., Kawate, T., Jingami, H., Kunishima, N., Ariyoshi, M., Kohda, D., Nakagawa, M., and Morikawa, K. (1999) Crystallographic and functional studies of very short patch repair endonuclease, *Mol. Cell 3*, 621−628.
9. Hickman, A. B., Li, Y., Mathew, S. V., May, E. W., Craig, N. L., and Dyda, F. (2000) Unexpected structural diversity in DNA recombination: the restriction endonuclease connection, *Mol. Cell 5*, 1025−1034.
10. Lovell, S., Goryshin, I. Y., Reznikoff, W. R., and Rayment, I. (2002) Two-metal active site binding of a Tn5 transposase synaptic complex, *Nat. Struct. Biol. 9*, 278−281.
11. Kvaratskhelia, M., George, S. J., Cooper, A., and White, M. F. (1999) Quantitation of metal ion and DNA junction binding to the Holliday junction endonuclease Cce1, *Biochemistry 38*, 16613−16619.
12. Bujacz, G., Alexandratos, J., Wlodawer, A., Merkel, G., Andrake, M., Katz, R. A., and Skalka, A. M. (1997) Binding of different divalent cations to the active site of avian sarcoma virus integrase and their effects on enzymatic activity, *J. Biol. Chem. 272*, 18161−18168.
13. Hadden, J. M., Declais, A. C., Phillips, S. E., and Lilley, D. M. (2002) Metal ions bound at the active site of the junction-resolving enzyme T7 endonuclease I, *EMBO J. 21*, 3505−3515.
14. Chevalier, B. S., and Stoddard, B. L. (2001) Homing endonucleases: structural and functional insight into the catalysts of intron/intein mobility, *Nucleic Acids Res. 29*, 3757−3774.
15. Horton, N. C., Newberry, K. J., and Perona, J. J. (1998) Metal ion-mediated substrate-assisted catalysis in type II restriction endonucleases, *Nat. Struct. Biol. 95*, 13489−13494.
16. Horton, J. R., and Cheng, X. (2000) PvuII endonuclease contains two calcium ions in active sites, *J. Mol. Biol. 300*, 1049−1056.
17. Viadiu, H., and Aggarwal, A. K. (1998) The role of metals in catalysis by the restriction endonuclease BamHI, *Nat. Struct. Biol. 5*, 910−916.
18. Lukacs, C. M., Kucera, R., Schildkraut, I., and Aggarwal, A. K. (2000) Understanding the immutability of restriction enzymes: crystal structure of BglII and its DNA substrate at 1.5 Å resolution, *Nat. Struct. Biol. 7*, 134−140.
19. Deibert, M., Grazulis, S., Sasnauskas, G., Siksnys, V., and Huber, R. (2000) Structure of the tetrameric restriction endonuclease NgoMIV in complex with cleaved DNA, *Nat. Struct. Biol. 7*, 792−799.
20. Newman, M., Lunnen, K., Wilson, G., Greci, J., Schildkraut, I., and Phillips, S. E. V. (1998) Crystal structure of restriction endonuclease Bg/I bound to its interrupted DNA recognition sequence, *EMBO J. 17*, 5466−5476.
21. Beese, L. S., and Steitz, T. A. (1991) Structural basis for the 3′−5′ exonuclease activity of *Escherichia coli* DNA polymerase I: a two metal ion mechanism, *EMBO J. 10*, 25−33.
22. Kostrewa, D., and Winkler, F. K. (1995) Mg^{2+} binding to the active site of EcoRV endonuclease: a crystallographic study of complexes with substrate and product DNA at 2 Å resolution, *Biochemistry 34*, 683−696.
23. Sam, M. D., and Perona, J. J. (1999) Catalytic roles of divalent metal ions in phosphoryl transfer by EcoRV endonuclease, *Biochemistry 38*, 6576−6586.
24. Sam, M. D., and Perona, J. J. (1999) Mn^{2+}-dependent catalysis by restriction enzymes: pre-steady-state analysis of EcoRV endonuclease reveals burst kinetics and the origins of reduced activity, *J. Am. Chem. Soc. 121*, 1444−1447.
25. Baldwin, G. S., Sessions, R. B., Erskine, S. G., and Halford, S. E. (1999) DNA cleavage by the EcoRV restriction endonuclease: roles of divalent metal ions in specificity and catalysis, *J. Mol. Biol. 288*, 87−103.
26. Pingoud, A., and Jeltsch, A. (2001) Structure and function of type II restriction endonucleases, *Nucleic Acids Res. 29*, 3705−3727.
27. Vipond, I. B., and Halford, S. E. (1995) Specific DNA recognition by EcoRV restriction endonuclease induced by calcium ions, *Biochemistry 34*, 1113−1119.
28. Martin, A. M., Horton, N. C., Lusetti, S., Reich, N. O., and Perona, J. J. (1999) Divalent metal dependence of site-specific DNA binding by EcoRV endonuclease, *Biochemistry 38*, 8430−8439.
29. Reid, S. L., Parry, D., Liu, H. H., and Connolly, B. A. (2001) Binding and recognition of GATATC target sequences by the EcoRV restriction endonuclease: a study using fluorescent oligonucleotides and fluorescence polarization, *Biochemistry 40*, 2484−2494.
30. Jeltsch, A., Alves, J., Wolfes, H., Maass, G., and Pingoud, A. (1993) Substrate-assisted catalysis in the cleavage of DNA by the EcoRI and EcoRV restriction enzymes, *Nat. Struct. Biol. 90*, 8499−8503.
31. Fuxreiter, M., and Osman, R. (2001) Probing the general base catalysis in the first step of BamHI action by computer simulations, *Biochemistry 40*, 15017−15023.
32. Jeltsch, A., Kroger, M., and Pingoud, A. (1995) Evidence for an evolutionary relationship among type-II restriction endonucleases, *Gene 160*, 7−16.
33. Bujnicki, J. M. (2000) Phylogeny of the restriction endonuclease-like superfamily inferred from comparison of protein structures, *J. Mol. Evol. 50*, 39−44.
34. Wilbanks, S. M., and McKay, D. B. (1995) How potassium affects the activity of the molecular chaperone Hsc70. II. Potassium binds specifically in the ATPase active site, *J. Biol. Chem. 270*, 2251−2257.
35. O'Brien, M. C., and McKay, D. B. (1995) How potassium affects the activity of the molecular chaperone Hsc70. I. Potassium is required for optimal ATPase activity, *J. Biol. Chem. 270*, 2247−2250.
36. Larsen, T. M., Laughlin, L. T., Holden, H. M., Rayment, I., and Reed, G. H. (1994) Structure of rabbit muscle pyruvate kinase complexed with Mn^{2+}, K^+, and pyruvate, *Biochemistry 33*, 6301−6309.
37. Viitanen, P. V., Lubben, T. H., Reed, J., Goloubinoff, P., O'Keefe, D. P., and Lorimer, G. H. (1990) Chaperonin-facilitated refolding of ribulosebisphosphate carboxylase and ATP hydrolysis by chaperonin 60 (groEL) are K^+ dependent, *Biochemistry 29*, 5665−5671.
38. Horton, N. C., Dorner, L. F., and Perona, J. J. (2002) Sequence selectivity and degeneracy of a restriction endonuclease mediated by DNA intercalation, *Nat. Struct. Biol. 9*, 42−47.
39. Kelly, T. J., Jr., and Smith, H. O. (1970) A restriction enzyme from *Haemophilus influenzae*. II, *J. Mol. Biol. 51*, 393−409.
40. Horton, N. C., Dorner, L. F., Schildkraut, I., and Perona, J. J. (1999) Crystallization and preliminary diffraction analysis of the

HincII restriction endonuclease−DNA complex, *Acta Crystallogr. D55*, 1943−1945.
41. Leslie, A. G. (1999) Integration of macromolecular diffraction data, *Acta Crystallogr. D55*, 1696−1702.
42. Evans, P. R. (1993) Data Reduction, *Proceedings of CCP4 Study Weekend*, pp 114−122, Daresbury Laboratory, Warrington, U.K.
43. Brünger, A. T., Adams, P. D., Clore, G. M., DeLano, W. L., Gros, P., Grosse-Kunstleve, R. W., Jiang, J. S., Kuszewski, J., Nilges, M., Pannu, N. S., Read, R. J., Rice, L. M., Simonson, T., and Warren, G. L. (1998) Crystallography & NMR system: A new software suite for macromolecular structure determination, *Acta Crystallogr. D54*, 905−921.
44. McRee, D. E. (1999) XtalView/Xfit: A versatile program for manipulating atomic coordinates and electron density, *J. Struct. Biol. 125*, 156−165.
45. Esnouf, R. M. (1999) Further additions to MolScript version 1.4, including reading and contouring of electron-density maps, *Acta Crystallogr. D55*, 938−940.
46. Kraulis, P. J. (1991) Molscript: A Program to Produce Both Detailed and Schematic Plots of Protein Structures, *J. Appl. Crystallogr. 24*, 946−950.
47. Merritt, E. A., and Murphy, M. E. P. (1994) Raster3d Version 2.0: A Program For Photorealistic Molecular Graphics, *Acta Crystallogr. D50*, 869−873.
48. Fried, M., and Crothers, D. M. (1981) Equilibria and kinetics of lac repressor-operator interactions by polyacrylamide gel electrophoresis, *Nucleic Acids Res. 9*, 6505−6525.
49. Taylor, J. D., Badcoe, I. G., Clarke, A. R., and Halford, S. E. (1991) EcoRV restriction endonuclease binds all DNA sequences with equal affinity, *Biochemistry 30*, 8743−8753.
50. Thielking, V., Selent, U., Köhler, E., Wolfes, H., Pieper, U., Geiger, R., Urbanke, C., Winkler, F. K., and Pingoud, A. (1991) Site-directed mutagenesis studies with EcoRV restriction endonuclease to identify regions involved in recognition and catalysis, *Biochemistry 30*, 6416−6422.
51. Martin, A. M., Sam, M. D., Reich, N. O., and Perona, J. J. (1999) Structural and energetic origins of indirect readout in site-specific DNA cleavage by a restriction endonuclease, *Nat. Struct. Biol. 6*, 269−277.
52. Grasby, J. A., and Connolly, B. A. (1992) Stereochemical outcome of the hydrolysis reaction catalyzed by the EcoRV restriction endonuclease, *Biochemistry 31*, 7855−7861.
53. Connolly, B. A., Eckstein, F., and Pingoud, A. (1984) The stereochemical course of the restriction endonuclease EcoRI-catalyzed reaction, *J. Biol. Chem. 259*, 10760−10763.
54. Cassano, A. G., Anderson, V. E., and Harris, M. E. (2004) Understanding the transition states of phosphodiester bond cleavage: insights from heavy atom isotope effects, *Biopolymers 73*, 110−129.
55. Strater, N., Lipscomb, W. N., Klabunde, T., and Krebs, B. (1996) Two-metal ion catalysis in enzymatic acyl- and phosphoryl-transfer reactions, *Angew. Chem., Int. Ed. Engl. 35*, 2024−2055.
56. Horton, N. C., Connolly, B. A., and Perona, J. J. (2000) Inhibition of EcoRV endonuclease by deoxyribo-3′-S-phosphorothiolates: A high-resolution X-ray crystallographic study, *J. Am. Chem. Soc. 122*, 3314−3324.
57. Perona, J. J., and Martin, A. M. (1997) Conformational transitions and structural deformability of EcoRV endonuclease revealed by crystallographic analysis, *J. Mol. Biol. 273*, 207−225.
58. Horton, N. C., and Perona, J. J. (2004) DNA cleavage by EcoRV endonuclease: two metal ions in three metal ion binding sites, *Biochemistry 43*, 6841−6857.
59. Bujnicki, J. M. (2000) Phylogeny of the restriction endonuclease-like superfamily inferred from comparison of protein structures, *J. Mol. Evol. 50*, 39−44.
60. Brenner, S. E., Chothia, C., and Hubbard, T. J. (1998) Assessing sequence comparison methods with reliable structurally identified distant evolutionary relationships, *Proc. Natl. Acad. Sci. U.S.A. 95*, 6073−6078.
61. Selent, U., Ruter, T., Kohler, E., Liedtke, M., Thielking, V., Alves, J., Oelgeschlager, T., Wolfes, H., Peters, F., and Pingoud, A. (1992) A site-directed mutagenesis study to identify amino acid residues involved in the catalytic function of the restriction endonuclease EcoRV, *Biochemistry 31*, 4808−4815.
62. Horton, N. C., Otey, C., Lusetti, S., Sam, M. D., Kohn, J., Martin, A. M., Ananthnarayan, V., and Perona, J. J. (2002) Electrostatic contributions to site specific DNA cleavage by EcoRV endonuclease, *Biochemistry 41*, 10754−10763.
63. Vipond, I. B., Baldwin, G. S., and Halford, S. E. (1995) Divalent metal ions at the active sites of the EcoRV and EcoRI restriction endonucleases, *Biochemistry 34*, 697−704.
64. Glusker, J. P. (1991) Structural aspects of metal liganding to functional groups in proteins, *Adv. Protein Chem. 42*, 1−76.
65. Maguire, M. E., and Cowan, J. A. (2002) Magnesium chemistry and biochemistry, *Biometals 15*, 203−210.
66. Kragten, J. (1978) *Atlas of metal−ligand equilibria in aqueous solution* (Horwood, E., Ed.) Halsted Press, Chichester, U.K.
67. Babu, C. S., Dudev, T., Casareno, R., Cowan, J. A., and Lim, C. (2003) A combined experimental and theoretical study of divalent metal ion selectivity and function in proteins: application to *E. coli* ribonuclease H1, *J. Am. Chem. Soc. 125*, 9318−9328.
68. Thorogood, H., Grasby, J. A., and Connolly, B. A. (1996) Influence of the phosphate backbone on the recognition and hydrolysis of DNA by the EcoRV restriction endonuclease. A study using oligodeoxynucleotide phosphorothioates, *J. Biol. Chem. 271*, 8855−8862.
69. Jeltsch, A., Pleckaityte, M., Selent, U., Wolfes, H., Siksnys, V., and Pingoud, A. (1995) Evidence for substrate-assisted catalysis in the DNA cleavage of several restriction endonucleases, *Gene 157*, 157−162.
70. Jen-Jacobson, L. (1997) Protein-DNA recognition complexes: conservation of structure and binding energy in the transition state, *Biopolymers 44*, 153−180.

BI0490082